IEEJ Journal of Industry Applications
Vol.1 No.1 pp.15–23 DOI: 10.1541/ieejjia.1.15

Paper

Sensorless Control of IPMSM: Past, Present, and Future

Seung-Ki Sul[*a)] Member, Sungmin Kim[*] Non-member

(Manuscript received Jan. 5, 2012, revised Feb. 24, 2012)

This paper presents the history of techniques used for sensorless control of the Interior Permanent Magnet Synchronous Machine (IPMSM) over the last 20 years. The techniques used in the first stage were based on the equivalent circuit of the IPMSM. They extracted rotor position information from the back EMF estimated through simple arithmetic. In the last 10 years, model reference adaptive control or observer-based control techniques have evolved and they have been used for the sensorless control of the IPMSM; however, the rotor position continues to be obtained from the back EMF. Simultaneously, sensorless control based on the magnetic saliency of the IPMSM has been achieved and commercialized. In this paper, an evaluation of the major techniques used for the sensorless control of the IPMSM has been presented, and their limitations have been clarified. Finally, the direction of future development of sensorless control is indicated.

Keywords: IPMSM, sensorless control

1. Introduction

Since the early 1980s, with the development of high-performance rare-earth permanent magnets, the Interior Permanent Magnet Synchronous Motor (IPMSM) has evolved. It was first used in high-performance servo drive and has recently been used in general-purpose industrial drives [(1)]. From the 1990s, because of the soaring of cost of electricity, the IPMSM has been considered as a candidate that could replace the induction motor. The induction machine has many merits, for example, it is mechanically robust, has low cost, is technically mature, and can be designed to have different speeds, torques, and shapes. However, because of the magnetizing current, its efficiency is poorer than that of a permanent-magnet-based motor, especially at a low load factor [(2)]. At the early stage of development of permanent magnet motor, Surface mounted Permanent Magnet Synchronous Motor (SPMSM) has been designed and applied to high performance servo application, where the control performance is the first concern. However, IPMSM has several merits compared to SPMSM, namely smaller size of magnet, easier detention of magnet, less eddy current in magnet, and possibility of flux weakening control [(3)]. Even though the control of the IPMSM is complex because of the reluctance torque associated with the saliency of the magnetic structure of the rotor, the IPMSM has been used in many industrial applications. In some applications, a general-purpose IPMSM has been used as the Surface-Mounted Permanent Magnet Synchronous Machine, where the d-axis current is set to be zero, for easier implementation of the control algorithm at the cost of the reluctance torque. Even under such a simple operating principle, the torque density of IPMSM is considerably higher than that of the general-purpose induction motor. The torque density per unit volume is 30% higher and the torque density per unit weight is 25% higher in the power range of several tens of kilowatt, for operation in near 1800 r/min. Further, the efficiency of the IPMSM is 7% higher than that of the high-efficiency premium induction motor and 10% higher than that of the standard general-purpose induction motor. Hence, recently, IPMSMs with ratings exceeding 500 hp have been used to replace the induction machine in general industrial applications such as hoist operation. However, in making the replacement, the position sensor of the IPMSM has been of concern [(4)]. Even though the IPMSM is mechanically robust and has a small size, the position sensor increases the axial length of the IPMSM and results in reduced torque density per unit volume. Furthermore, the sensor can adversely affect the robustness of the IPMSM, both electrically and mechanically. To overcome these problems, position sensorless drive techniques for the IPMSM have been studied over the last two decades, and some of them have been commercialized and used for industrial purposes [(5)(6)]. Still, the performance of the sensorless drive of the IPMSM is limited. Some commercialized techniques had shown reasonable performances in overall operating conditions except low speed/low frequency region. For last ten years, sensorless drive techniques based on high frequency signal injection methods have been evolved. Those techniques can guarantee the reasonable torque control performance even at zero speed/zero frequency. An overview of the sensorless control techniques of the IPMSM developed for last two decades are described in this paper, and the merit and the demerit of typical technique are discussed. Based on the discussion, the direction of future development of sensorless control technique for the IPMSM could be enlightened.

2. Past

The sensorless control of the IPMSM had been studied for

a) Correspondence to: Seung-Ki Sul. E-mail: sulsk@plaza.snu.ac.kr
* Seoul National University Power Electronics Center (SPEC), Department of Electrical Engineering and Computer Science, Seoul National Univeristy
599, Gwanangno, Gwanak-gu, Seoul 151-744, Korea

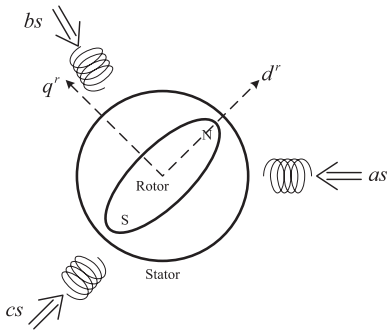

Fig. 1. Analytical model of Interior Permanent Magnet Synchronous Machine

several decades but the major publications have been reported from early of 1990's [7][8]. The information of the rotor position is included in the back EMF as shown in Fig. 1.

The back EMF can be calculated in the stationary frame model of the IPMSM or in the estimated rotor reference frame. The technique based on back EMF presents good performance in the middle and high speed operating region of the IPMSM. And it is commercialized by many companies. The performance above 10% of the rated speed with rated load in motoring and generating operation is quite satisfactory and acceptable for the most of low end drive application. The bandwidth of the speed regulation loop can be extended more than several Hz. However, at standstill or very low rotating speed, because the magnitude of the back EMF is proportional to the rotating speed, the signal is too weak to be used as the position information and the signal is easily contaminated by the measurement noises or the nonlinear effects of PWM inverter. To enhance the performance of the sensorless control at lower operating speed, Model Reference Adaptive Control (MRAC) and/or closed observer has been applied [9][10]. And simultaneously, several careful dead time compensation methods had been incorporated [11][12]. With these refinements the controllable speed can be down to a few percent of the rated speed and the control bandwidth can be extended up to 10 Hz.

All back EMF based sensorless control techniques are based on the following voltage equation of the IPMSM.

$$\left.\begin{aligned} v_{ds}^{\hat{r}} &= R_s i_{ds}^{\hat{r}} + L_{ds}\frac{di_{ds}^{\hat{r}}}{dt} - \hat{\omega}_r L_{qs} i_{qs}^{\hat{r}} - \hat{\omega}_r \lambda_f \sin\tilde{\theta}_r \\ v_{qs}^{\hat{r}} &= R_s i_{qs}^{\hat{r}} + L_{qs}\frac{di_{qs}^{\hat{r}}}{dt} + \hat{\omega}_r L_{ds} i_{ds}^{\hat{r}} + \hat{\omega}_r \lambda_f \cos\tilde{\theta}_r \end{aligned}\right\} \cdots\cdots (1)$$

where the voltages and currents are measured in the estimated rotor reference frame. And the error between the real rotor position and the estimated rotor position is defined by (2) as shown in Fig. 2.

$$\tilde{\theta}_r = \theta_r - \hat{\theta}_r \cdots\cdots (2)$$

$$\begin{aligned} \hat{e}_{ds}^{\hat{r}} &= -\hat{\omega}_r \lambda_f \sin\tilde{\theta}_r \approx v_{ds}^{\hat{r}} - R_s i_{ds}^{\hat{r}} + \hat{\omega}_r L_{qs} i_{qs}^{\hat{r}} \\ \hat{e}_{qs}^{\hat{r}} &= \hat{\omega}_r \lambda_f \cos\tilde{\theta}_r \approx v_{qs}^{\hat{r}} - R_s i_{qs}^{\hat{r}} - \hat{\omega}_r L_{ds} i_{ds}^{\hat{r}} \end{aligned} \cdots\cdots (3)$$

Under the assumption of the steady-state operation, the back EMF voltage can be estimated simply by (3). Then,

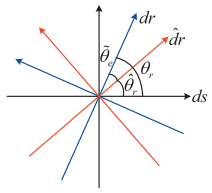

Fig. 2. Voltage plane in stationary frame, rotor reference frame, and estimated rotor reference frame

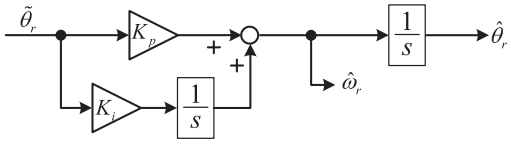

Fig. 3. Angle error correction controller based on PI regulator

the position error can be directly derived as (4).

$$\tilde{\theta}_r = \tan^{-1}\left(\frac{\hat{\omega}_r \lambda_f \sin\tilde{\theta}_r}{\hat{\omega}_r \lambda_f \cos\tilde{\theta}_r}\right) \cdots\cdots (4)$$

Because of the assumption of the steady state ignoring the variation of current, this direct calculation is not suitable to estimate the position error when the current varies rapidly according to the load torque disturbance or torque reference change. Hence, the control bandwidth is limited. This shortcoming can be lessened by employing the closed loop state observer [13]. From (1), under the assumption of slow enough variation of back EMF at the estimated rotor reference frame, a state equation augmenting back EMF voltage, $\hat{e}_{ds}^{\hat{r}}$, $\hat{e}_{qs}^{\hat{r}}$ can be formulated as (5) and (6). And the angle error can be obtained as like (4).

$$\begin{aligned} \dot{\hat{x}} &= A\hat{x} + Bu + L(y - c\hat{x}) \\ &= \begin{bmatrix} -\frac{R_s}{L_{ds}} & \frac{\hat{\omega}_r L_{qs}}{L_{ds}} & \frac{1}{L_{ds}} & 0 \\ \frac{-\hat{\omega}_r L_{ds}}{L_{qs}} & -\frac{R_s}{L_{qs}} & 0 & \frac{1}{L_{qs}} \\ 0 & 0 & 0 & 0 \\ 0 & 0 & 0 & 0 \end{bmatrix} \begin{bmatrix} \hat{i}_{ds}^{\hat{r}} \\ \hat{i}_{qs}^{\hat{r}} \\ \hat{e}_{ds}^{\hat{r}} \\ \hat{e}_{qs}^{\hat{r}} \end{bmatrix} \\ &\quad + \begin{bmatrix} \frac{1}{L_{ds}} & 0 \\ 0 & \frac{1}{L_{qs}} \\ 0 & 0 \\ 0 & 0 \end{bmatrix} \begin{bmatrix} v_{ds}^{\hat{r}} \\ v_{qs}^{\hat{r}} \end{bmatrix} + L(y - \hat{y}) \end{aligned} \cdots\cdots (5)$$

$$\hat{y} = \begin{bmatrix} \hat{i}_{ds}^{\hat{r}} \\ \hat{i}_{qs}^{\hat{r}} \end{bmatrix} = \begin{bmatrix} 1 & 0 & 0 & 0 \\ 0 & 1 & 0 & 0 \end{bmatrix} \hat{x} = C\hat{x} \cdots\cdots (6)$$

Also, the direct update of angle error is vulnerable to measurement noise and parameter errors. And the estimated rotor angle can be updated through angle error correction controller based on PI regulator as shown in Fig. 3, where the rotational speed can be obtained as a byproduct. The controller is a kind of the state filter.

These back EMF based sensorless methods estimate the rotor position and speed from the stator voltage and currents. With these basic ideas, many different implementation

techniques have been reported. Some are based on the estimation of the back EMF voltage from the permanent magnet flux linkage using a state observer or a Kalman filter [14][15]. Others use the voltage or current error between the measured values and the calculated values in the estimated rotor position [16]–[18]. In Ref. (16), the concept of an Extended EMF is proposed to simplify the estimation of the back EMF. By applying the Extended EMF concept, many approximations to estimate the back EMF are eliminated. Because of the difference of d-axis inductance and q-axis inductance of the IPMSM, the voltage equation in the estimated rotor reference frame is complex. While, with Extended EMF, all inductance saliency related terms are moved to the Extended EMF terms in voltage equations. Then the modified voltage equation in the estimated rotor reference frame can be simple and the sensorless algorithm can be applied easily. The modified voltage equation can be described as (7) with Extended EMF such as (8) at real rotor position:

$$v_{ds}^r = R_s i_{ds}^r + L_{ds}\frac{di_{ds}^r}{dt} - \omega_r L_{qs} i_{qs}^r$$
$$v_{qs}^r = R_s i_{qs}^r + L_{ds}\frac{di_{qs}^r}{dt} + \omega_r L_{qs} i_{ds}^r + E_{ex} \quad \cdots\cdots\cdots\cdots (7)$$

$$E_{ex} = \omega_r\left[\left(L_{ds} - L_{qs}\right) i_{ds}^r + \lambda_f\right] - \left(L_{ds} - L_{qs}\right)\frac{di_{qs}^r}{dt} \quad \cdots\cdots\cdots\cdots\cdots (8)$$

In a different approach, the estimated voltage/current difference with the actual voltage/current can be used for extracting the position error [17]. If the model is exact with the actual motor, the voltage and/or current can be calculated exactly. However, if there are differences between the actual voltage and/or current and the calculated ones based on the model, it can be understood that there is the position error between the actual position and the estimated position. Therefore, from the voltage and/or current difference, the position error can be estimated. This method can be implemented based on the machine voltage model and the machine current model, respectively. In the voltage model, the calculated voltage based on the voltage model is compared with the voltage reference of the current control loop. The difference between the calculated voltage and the voltage reference can be used as a position correction value as Fig. 4(a). In the current model, the calculated current and the measured current are compared to get the position error values as Fig. 4(b). These error values can be used as correction value to the state filter or observer.

Unlike the back EMF estimation or model based methods, the voltage reference of current controller can be directly used as the position error related values [18]. In these machine model based sensorless techniques, the machine parameters such as resistance, inductance, and the permanent magnet flux linkage have critical effects on the position estimation performance.

Even though there are so many variations of sensorless control techniques based on back EMF voltage for the IPMSM, the techniques can be represented as a block diagram in Fig. 5. The design of each block might be different according to the specific sensorless control technique. And, the performance of each technique may be different.

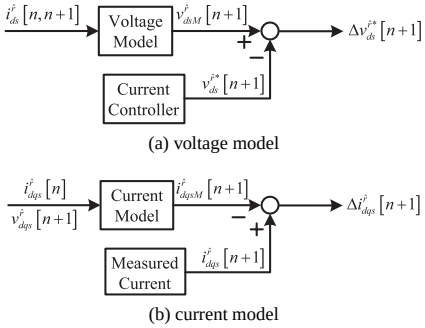

(a) voltage model

(b) current model

Fig. 4. Block diagram of voltage and current model based sensorless control

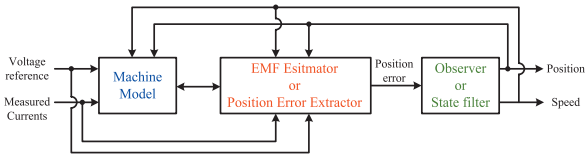

Fig. 5. Representative block diagram of sensorless control technique based on Back EMF

But, theoretically, all techniques would not work at zero frequency, where back EMF does not exist. Practically, in the case of a few kW or above rated power of the IPMSM, because back EMF is always estimated from the terminal voltage and current information, the technique would not work at lower than 1% of the rated speed even with careful parameter adaptation and dead time compensation. In the most of applications of drive where the induction motor was replaced by the IPMSM, torque and speed control range down to a few percents of the rated speed would be enough. However, some application where speed and/or torque should be controlled absolutely from standstill, that is, zero speed, the back EMF based techniques cannot be used.

3. Present

The rotor position of the IPMSM can be estimated from the characteristics of the IPMSM: the spatial inductance distribution is determined by the rotor position because of the saliency of the magnetic path of d and q axis as shown in Fig. 6. The saliency comes from the difference of magnetic permeability of the core and permanent magnet.

To extract the spatial inductance variation, the relationship between current and voltage can be employed. To examine the current-voltage relationship, PWM current ripple can be used [19]–[22]. By measuring current variation according to the voltage vector variation in a PWM period, inductance can be calculated directly [19]–[21] or estimated with a non-linear estimator [22]. However, these techniques require the modification of PWM switching pattern, because the current variation in the conventional SVPWM is too small to be used for the calculation of the inductance. And additional devices to measure the phase currents in arbitrary time should be designed in control hardware, which might not be acceptable to many industry applications. Similarly, the intended discontinuous voltage signal injected method has been proposed [23]. In Ref. (23), large voltage signal is injected for very short time interval and the current variation by the injected voltage signal is measured. From measured current variation, the

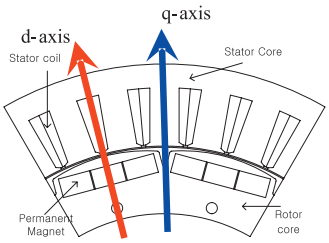

Fig. 6. Typical lay-out of the IPMSM and d-q axis of rotor reference frame

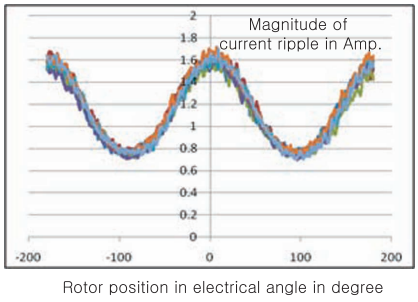

Fig. 7. Magnitude of current ripple according to the injected continuous high frequency pulsating sinusoidal voltage signal at different rotor position to the stator

inductance and rotor position can be estimated. From this method, however, the rotor position information can be discontinuously obtained, and the rotor position estimation and the overall control performance could be degraded.

From the late of 1990's, the continuous signal injection methods without PWM modification have been proposed, and the signal can be easily augmented into the conventional current control loop [24]–[31]. The continuous voltage signals into the IPMSM causes the current ripple, which reflects rotor position as shown in Fig. 7.

From the corresponding current ripple, the rotor position information can be extracted with a properly designed observer and/or a state filter. For each signal injection sensorless method, demodulation process should be incorporated to extract the rotor position related value from current ripple. These continuous signal injection sensorless methods can be further classified into two categories according to where the signal is injected: the rotating voltage signal injection in the stationary reference frame [24]–[30] and the pulsating voltage signal injection in the estimated rotor reference frame [24]–[29]. The rotating voltage signal technique injects the continuous voltage signal spatially regardless of the rotor position, and the pulsating voltage signal technique injects the continuous pulsating voltage signal on the estimated rotor position. The pulsating signal injection technique is more robust to local saliency, which may occur from the design of the IPMSM, especially in the case of concentrated winding. Moreover, the loss of the pulsating signal injection due to the injected signal is a half of that of the rotating voltage signal method, and the temperature of the magnet of the motor would be lower in pulsating signal injection [32]–[34].

If the pulsating voltage signal is injected into the exact d-axis rotor reference frame, q-axis current ripple due to the injected voltage does not happen. However, because the exact rotor position is not available, the injection voltage signal

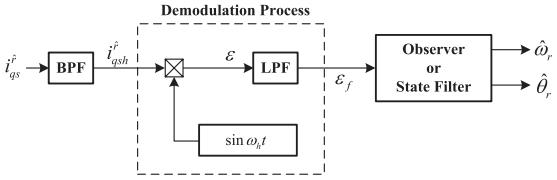

Fig. 8. Block diagram of the heterodyning demodulation process

actually differs from the ideal injection voltage. The injection voltage in the estimated rotor reference frame can be rewritten with consideration of the estimated rotor position error as (9).

$$v_{dqsh}^{\hat{r}*} = V_{inj}\begin{bmatrix}\cos\omega_h t\\ 0\end{bmatrix} \cdots\cdots (9)$$

Considering the position error, the actual injection voltage signal into the real rotor reference frame can be described as (10).

$$v_{dqsh}^{r} = T\left(\tilde{\theta}_r\right) v_{dqsh}^{\hat{r}*} = V_{inj}\begin{bmatrix}\cos\tilde{\theta}_r\cos\omega_h t\\ -\sin\tilde{\theta}_r\cos\omega_h t\end{bmatrix} \cdots\cdots (10)$$

where $T\left(\tilde{\theta}_r\right)$ stands for the transformation from estimated rotor reference frame to real rotor reference frame. Then, the corresponding current response in the estimated rotor reference frame can be deduced as (11).

$$\begin{bmatrix}i_{dsh}^{\hat{r}}\\ i_{qsh}^{\hat{r}}\end{bmatrix} = T\left(\tilde{\theta}_r\right)^{-1}\begin{bmatrix}i_{dsh}^{r}\\ i_{qsh}^{r}\end{bmatrix} = \frac{V_{inj}}{\omega_h}\begin{bmatrix}\left(\dfrac{\cos^2\tilde{\theta}_r}{L_{ds}}+\dfrac{\sin^2\tilde{\theta}_r}{L_{qs}}\right)\sin\omega_h t\\ \dfrac{1}{2}\left(\dfrac{-\Delta L}{L_{ds}L_{qs}}\right)\sin 2\tilde{\theta}_r\sin\omega_h t\end{bmatrix} \cdots\cdots (11)$$

As it can be seen from (11), the rotor position error is placed in the estimated q-axis current response. To separate the position error from the estimated q-axis current response, demodulation processes have been employed generally. Among the various demodulation processes, the heterodyning demodulation process is the most well known method [24]. Fig. 8 shows the simple heterodyning demodulation process. Using this process, the position error can be extracted from the q-axis current response. The final result of the demodulation process from the method in Fig. 8, ε_f, can be derived as (12) under the assumption that the error between the real rotor position and the estimated one is small.

$$\varepsilon_f \approx \frac{1}{2}\frac{V_{inj}}{\omega_h}\left(\frac{-\Delta L}{L_{ds}L_{qs}}\right)\left(\theta_r-\hat{\theta}_r\right) \cdots\cdots (12)$$

And, the demodulation process result, ε_f, can be used as a corrective error input to observer or state filter in Fig. 9. One of the typical implementations of the block diagram in Fig. 9, which had been commercialized, is shown in Fig. 10 [26]. In this implementation, the measurement axis was introduced and the current at this axis was used for the demodulation. A simple PI type state filter was used instead of observer as an angle correction controller.

In this technique, because of number of filters, namely low

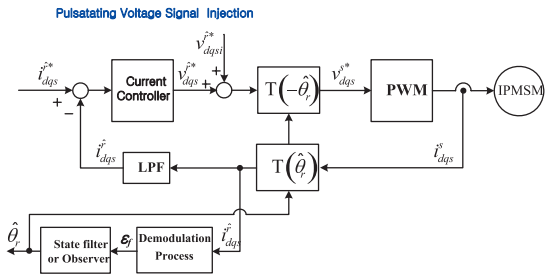

Fig. 9. Control block diagram of general pulsating signal injection techniques

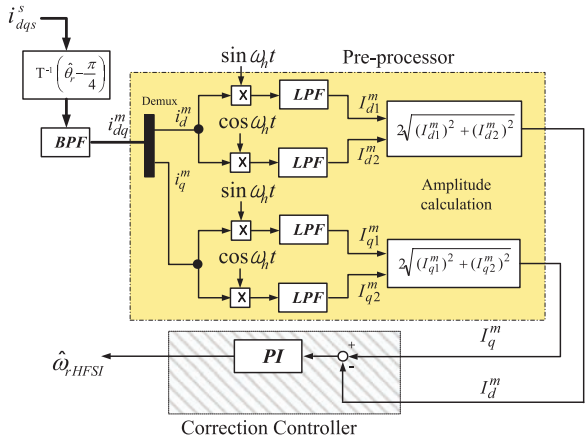

Fig. 10. Control block diagram of pulsating signal injection technique

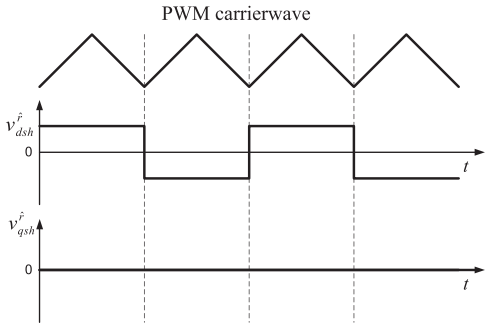

Fig. 11. Triangular carrier wave and square wave injected signal at estimated d axis

pass filters, and band pass filter, the tuning of the filters are difficult and the control bandwidth is limited due to the signal delays of the filters. With this implementation, the speed control bandwidth has been limited to less than 10 Hz in the case of general purpose IPMSM drive.

To improve the speed control bandwidth, a different implementation method has been reported [27]–[29]. A square wave signal was injected synchronously to the triangular carrier wave of PWM of inverter as shown in Fig. 11, and the injection frequency was increased up to a half of switching frequency. With the injected signal, the current in the stationary d and q axis reference frame can be represented as (13).

$$\begin{bmatrix} i^s_{dsh} \\ i^s_{qsh} \end{bmatrix} \approx \begin{bmatrix} \dfrac{1}{L_{ds}\omega_h}\cos(\theta_r)\sin\omega_h t \\ \dfrac{1}{L_{ds}\omega_h}\sin(\theta_r)\sin\omega_h t \end{bmatrix} \quad \left(\because\ \tilde{\theta}_r \approx 0\right) \cdots\cdots\cdots\cdots\cdots\cdots (13)$$

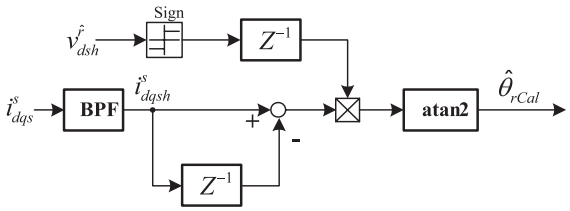

Fig. 12. Demodulation process with the square wave signal injection

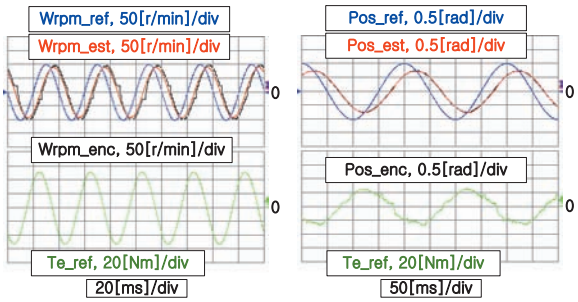

(a) Speed control (b) Position control

Fig. 13. Speed and position control performance with the square signal injection to estimated d axis (11 kW 6 pole general purpose IPMSM)

With the injection signal in Fig. 11, the demodulation process can be simplified as shown in Fig. 12 and there is no low pass filter. On the top of easy tuning of the controller, the speed control bandwidth with this technique can be extended up to 25 Hz as shown in Fig. 13(a) with an off-the-shelf 11 kW general purpose IPMSM thanks to no signal delay of low pass filters. The estimated speed (Wrpm_est) through the injected signal tracks the reference speed (Wrpm_ref) better than the speed from encoder (Wrpm_enc) at near zero speed. The speed from encoder has bumps at near zero speed due to the limited number of pulse per revolution (1024 pulses in here) and the sampling time (1 ms in here). From Fig. 13(b), the position control bandwidth can be understood as 5 Hz.

The signal injection technique is effective for position and speed estimation in ultra-low speed region including zero stator frequency. However, due to the signal injection, the torque ripple and the acoustic noise at the injected signal frequency are inevitable. Furthermore, the additional voltage to inject the signal, which may be several tens of percent of the rated voltage of the IPMSM, would be prohibitive in the medium or higher speed operation region of the IPMSM where the voltage from PWM inverter is already near rated value. As mentioned in chapter 2 of this paper, because the back EMF based technique is able to estimate position and speed without acoustic and additional torque ripple above 10% of the rated speed, a hybrid method can be employed as shown in Fig. 14, where the high frequency signal injection (HFSI) technique is used at lower speed and back EMF technique at higher speed [35]. The key idea in here is the changeover which is done only based on the internal speed $\hat{\omega}_{cmb}$. The internal speed $\hat{\omega}_{cmb}$ consists of the estimated speed of both techniques. The internal estimated speed is set as (14).

$$\hat{\omega}_{cmb} = \hat{\omega}_0 + G_1 \cdot \hat{\omega}_{BEMF} + G_2 \cdot \hat{\omega}_{HFSI} \cdots\cdots\cdots (14)$$

where $\hat{\omega}_0$ is given by direct calculation from estimated back EMF voltage, $\hat{\omega}_{BEMF}$ is a kind of the correction control term

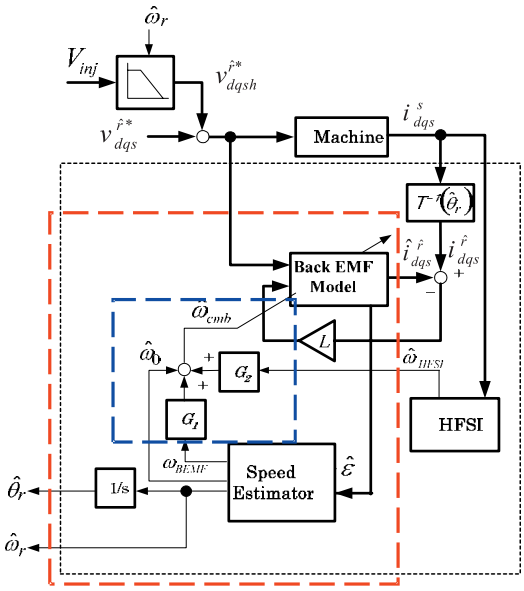

Fig. 14. Position and speed estimator with a hybrid method

to make the angle error $\hat{\varepsilon}$ null, and G_1 and G_2 are weighting factors. The weighting factors are regulated along with the command and/or the estimated speed. The internal estimated speed $\hat{\omega}_{cmd}$ is only employed in the machine model of the back EMF based method, and not employed to estimate the position of the magnet flux. The position is estimated by integration of the estimated speed $\hat{\omega}_r$.

To get the rated torque with rated current at starting, the initial position should be identified. The variation of the magnitude of the ripple current due to inductance variation shown in Fig. 7 reveals symmetry to the d axis in a half period of rotor position. So, d axis (north pole of magnet) and −d axis (south pole of magnet) in rotor reference frame of the IPMSM cannot be differentiated from the variation of the magnitude of the current ripple. So, another technique is needed for the starting of the IPMSM with rated torque at rated current. The north pole and south pole can be identified with the characteristic of the magnetic saturation of the core due to the flux linkage from the permanent magnet [36][37].

The d-axis second harmonic component of injected frequency has polarity information as (15).

$$\varepsilon_{pol} \equiv LPF\left(i^{\hat{r}}_{dsh}\cos 2\omega_h t\right) \cdots\cdots\cdots\cdots\cdots\cdots\cdots\cdots (15)$$

where *LPF* stands for Low Pass Filtering process and the cut off frequency of the filter is one order less than injected signal frequency. The injected signal is shown in Fig. 15 and a block diagram of the signal processing for initial pole position identification is shown in Fig. 16. With this technique the initial pole position can be identified within 100 ms [28].

Generally, the frequency of injected voltage signal is determined between the current control bandwidth and the PWM switching frequency. As the frequency of the injected signal is getting higher, the dynamics of the sensorless control can be enhanced and the interference between the injected signal and the fundamental components of the current control can be diminished [30]. If the PWM switching frequency is near or above the audible frequency range, the acoustic noise by injected signal can be remarkably reduced or totally

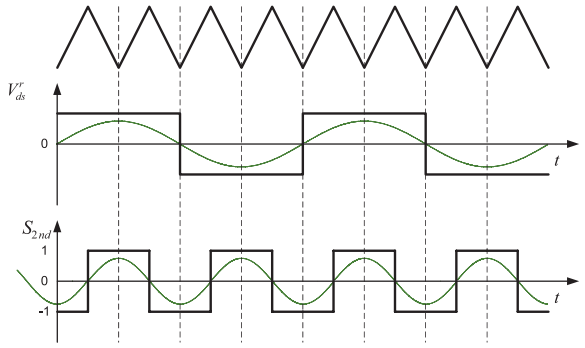

Fig. 15. Injected signal and second other harmonic signal for initial position identification

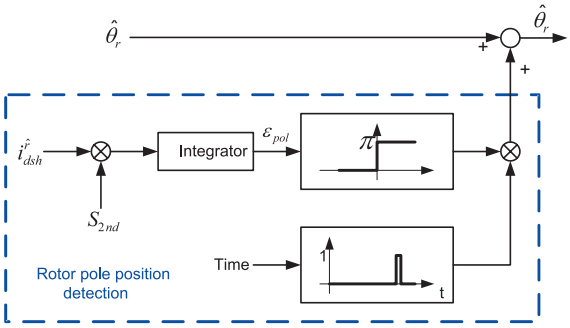

Fig. 16. Block diagram of signal processing for initial pole position identification

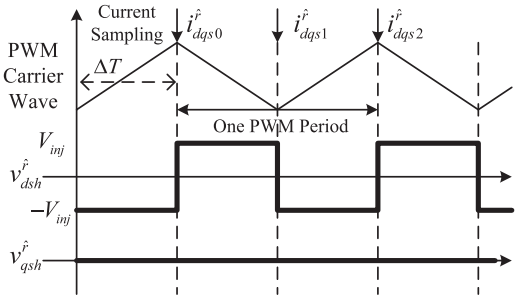

Fig. 17. Pulsating injection voltage signal in the estimated rotor reference frame. In a PWM period, three successively measured currents are used to estimate the rotor position

eliminated. To reduce the acoustic noise, a signal injection technique whose frequency is PWM switching frequency has been proposed [31]. The injected voltage is shown in Fig. 17. In this technique, the sampling of the current and updating PWM is done twice in a PWM switching period. And, the sampling period, ΔT, is a half of PWM switching period. The difference between successively sampled currents at the estimated rotor reference frame has rotor position information as seen from (16).

$$\begin{bmatrix}\Delta i^{\hat{r}}_{dsh}\\ \Delta i^{\hat{r}}_{qsh}\end{bmatrix} = T\left(\tilde{\theta}_r\right)^{-1}\begin{bmatrix}\Delta i^{r}_{dsh}\\ \Delta i^{r}_{qsh}\end{bmatrix}$$
$$= \pm\Delta T\cdot V_{inj}\begin{bmatrix}\dfrac{\cos^2\tilde{\theta}_r}{L_{ds}}+\dfrac{\sin^2\tilde{\theta}_r}{L_{qs}}\\ \dfrac{1}{2}\left(\dfrac{1}{L_{ds}}-\dfrac{1}{L_{qs}}\right)\sin 2\tilde{\theta}_r\end{bmatrix} \cdots\cdots (16)$$

Especially, q axis current can be used as the input of the

demodulation process, ε_f, as shown in Fig. 18. Thanks to the development of IGBT and DSP technology, the switching frequency of recently announced PWM inverter can be over 16 kHz, which is near the limit of human audible range. With this injection frequency, the audible noise can be virtually eliminated at the cost of larger magnitude of injection voltage and a little increased loss due to the higher frequency injected signal. As shown in Fig. 19, with this signal injection technique, the electric rotor position error is less than 0.3 rad, which means less than 0.1 rad error in mechanical angle without any position compensation in the case of 11 kW, 6 pole, general purpose IPMSM. With careful compensation according to the torque and speed, the position error can be reduced further.

With specially designed IPMSM for sensorless control, the speed and position control bandwidth can be extended more than 50 Hz and 10 Hz, respectively as shown in Fig. 20. The flux density of the specially designed IPMSM is reduced and it reveals better sinusoidal inductance variation according to the rotor position at the cost of reduced torque density [38].

As the machine design technology developed, the SPMSM which has inherently the isotropic inductance characteristics can be also used for signal injection sensorless control. In Refs. (39) (40), the inherent or inserted stator or rotor bridges in structurally symmetric machines generate saliency and can be also used for sensorless control. In Ref. (41), machine spatial saliency is analyzed with zigzag leakage flux concept and the machine design rules for generating the inductance saliency in the SPMSM was proposed.

With the introduction of commercial sensorless drive enabling zero speed operation, many IPMSM drives with position sensor have been replaced with the sensorless drive. One of the typical examples is lift application, where the torque control at zero speed to prevent roll back and shock at the starting of the cage of the lift is prerequisite. And in other applications where higher starting torque and less acceleration time are key requirements, namely oil injected screw compressor and injection molding machine, the sensorless drives increase reliability and reduce cost [42].

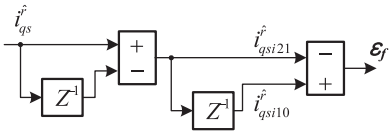

Fig. 18. Demodulation process with PWM switching frequency signal injection

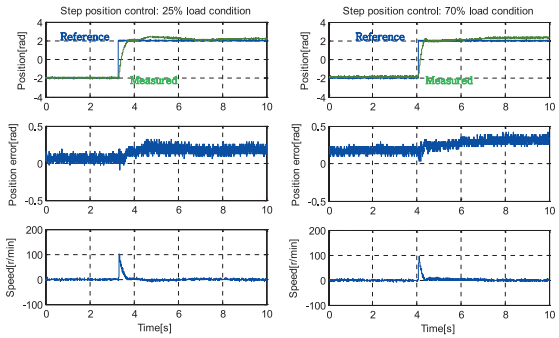

(a) Position control (25% load) (b) Position control (70% load)

Fig. 19. Electric rotor position control with 11 kW, 6 pole general purpose IPMSM. Electric rotor position reference varies from −2 rad to 2 rad. (a) 25% load condition (b) 70% load condition

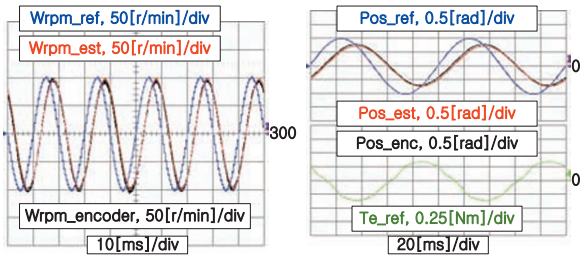

(a) Speed control (b) Position control

Fig. 20. Speed and position control performance with specially designed IPMSM for sensorless control (80 W 6 pole IPMSM)

4. Future

Though the sensorless control techniques has been evolved remarkably for last decades and the performance of the sensorless drive is comparable to low end servo where the resolution of encoder is less than a few hundreds per revolution, there are still number of problems to be solved. In some IPMSMs, especially the machine with higher torque density and wide flux weakening range, the variation of the inductance according to the rotor position is not sinusoidal and the position where minimum inductance occurs are moving according to the stator current as shown in Fig. 21. This phenomenon comes in many different forms. The position error

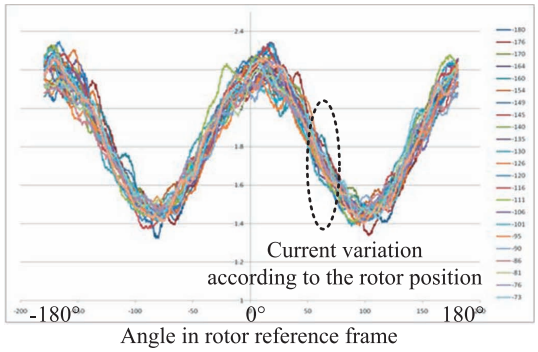

(a) no load condition

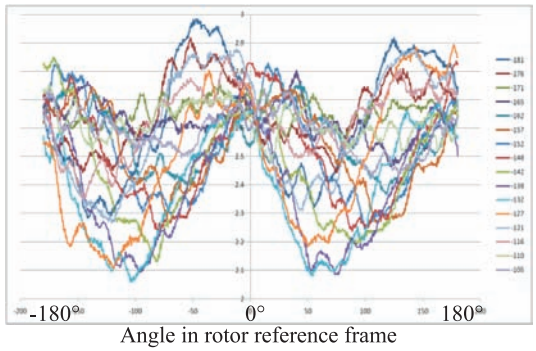

(b) 100% load condition

Fig. 21. Magnitude of current ripple according to the injected continuous high frequency pulsating sinusoidal voltage signal at different rotor position to the stator (25 kW, concentrated winding, IPMSM for electric vehicle traction application)

between the real position and the estimated position has 2nd, 6th, etc harmonics by this flux saturation [43][44]. The flux density of the IPMSM in the figure is increased to get higher torque density and the stator employs concentrated winding to reduce axial length of the motor. The sensorless drive with this type of the IPMSM is formidable target to achieve.

Though the control bandwidth has been improved several fold in the last decade, to apply the sensorless drive to high grade control purpose, the bandwidth should be improved at least a few times more. To achieve this control bandwidth, the design of the IPMSM itself and all signal processing techniques especially careful compensation of all nonlinearity of PWM inverter and measurement system should be incorporated simultaneously [45].

With the high frequency signal injection, the rotor position can be identified from standstill. However, because the identified position is in electrical angle, the absolute position of the rotor is not yet identified except 2 poles IPMSM, which is rarely used in the field. For some application such as tool changer or robot manipulator, absolute position information of the rotor is prerequisite. In this case, still the identification and control of the absolute position of the rotor is an open question. The special design of the rotor and stator of the IPMSM together with novel signal processing technology might open new horizon of the sensorless control of the IPMSM in absolute positioning.

References

(1) D.W. Novotny and T.A. Lipo: "Vector control and dynamics of AC drives", Clarendon Press, Oxford (1996)

(2) H. Murakami, Y. Honda, H. Kiriyama, S. Morimoto, and Y. Taketa: "The performance comparison of SPMSM, IPMSM and SynRM in use as air-conditioning compressor", in Proc. IEEE IAS Annual Meeting, pp.840–845 (1999)

(3) K. Akatsu, K. Narita, Y. Sakashita, and T. Yamada: "Characteristics comparison between SPMSM and IPMSM under high flux density condition by both experimental and analysis results", in Proc. ICEMS, pp.2848–2853 (2008)

(4) P. Vas: "Sensorless vector and direct torque control", Oxford (1998)

(5) G. Lee, W.-J. Lee, J. Ahn, and D. Cheong: "A simple sensorelss algorithm for an interior permanent magnet synchronous motor using a flux observer.pdf", in Proc. of ICPE2011-ECCE Asia (2011)

(6) P.P. Acarnley and J.F. Watson: "Review of position-sensorless operation of brushless permanent-magnet machines", IEEE Trans. Ind. Electron., Vol.53, No.2, pp.352–362 (2006-4)

(7) M. Schroedl: "Operation of the permanent magnet synchronous machine without a mechanical sensor", in Proc. Power Electronics and Variable-Speed Drives, pp.51–56 (1990)

(8) N. Matsui, T. Takeshita, and K. Yasuda: "A new sensorless drive of brushless DC motor", in Proc. IEEE IECON'92, pp.430–435 (1992)

(9) R.B. Sepe and J.H. Lang: "Real-time observer-based (adaptive) control of a permanent-magnet synchronous motor without mechanical sensors", IEEE Trans. Ind. Applicat., Vol.28, No.6, pp.1345–1352 (1992-11/12)

(10) A. Piippo, M. Hinkkanen, and J. Luomi: "Analysis of an adaptive observer for sensorless control of interior permanent magnet synchronous motors", IEEE Trans. Ind. Electron., Vol.55, No.2, pp.570–576 (2008-2)

(11) N. Hur, K. Hong, and K. Nam: "Sensorless vector control in the presence of voltage and current measurement errors by dead-time", in Proc. IEEE IAS Annual Meeting, pp.433–438 (1997)

(12) Y. Inoue, K. Yamada, S. Morimoto, and M. Sanada: "Effectiveness of voltage error compensation and parameter identification for model-based sensorless control of IPMSM", IEEE Trans. Ind. Applicat., Vol.45, No.1, pp.213–221 (2009-1/2)

(13) Y.-C. Son, B.-H Bae, and S.-K Sul: "Sensorless operation of permanent magnet motor using direct voltage sensing circuit", in Proc. IEEE IAS, pp.1674–1678 (2002)

(14) Y.-R. Kim, S.-K. Sul, and M.-H. Park: "Speed sensorless vector control of induction motor using extended Kalman filter", IEEE Trans. Ind. Applicat., Vol.30, No.5, pp.1225–1233 (1994-9/10)

(15) S. Bolognani, L. Tubiana, and M. Zigliotto: "Extended Kalman filter tuning in sensorless PMSM drives", IEEE Trans. Ind. Applicat., Vol.39, No.6, pp.1741–1747 (2003-11/12)

(16) S. Morimoto, K. Kawamoto, M. Sanada, and Y. Takeda: "Sensorless control strategy for salient-pole PMSM based on extended EMF in rotating reference frame", IEEE Trans. Ind. Appl., Vol.38, No.4, pp.1054–1061 (2002-7/8)

(17) N. Matsui: "Sensorless operation of brushless DC motor drives", in Proc. IEEE IECON'93, pp.739–744 (1993)

(18) B.-H. Bae, S.-K. Sul, J.-H. Kwon, and J.-S. Byeon: "Implementation of sensorless vector control for super-high-speed PMSM of turbo-compressor", IEEE Trans. Ind. Applicat., Vol.39, No.3, pp.811–818 (2003-5/6)

(19) A.B. Kulkarni and M. Ehsani: "A novel position sensor elimination technique for the interior permanent-magnet synchronous motor drive", IEEE Trans. Ind. Applicat., Vol.28, No.1, pp.144–170 (1992-1/2)

(20) S. Ogasawara and H. Akagi: "Implementationand position control performance of a position-sensorless IPM motor drive system based on magnetic saliency", IEEE Trans. Ind. Applicat., Vol.34, pp.806–812 (1998-7/8)

(21) M. Mamo, K. Ide, M. Sawamura, and J. Oyama: "Novel rotor position extraction based on carrier frequency component method (CFCM) using two reference frames for IPM drives", IEEE Trans. Ind. Electron., Vol.52, No.5, pp.508–514 (2005-4)

(22) V. Petrovic, A.M. Stankovic, and V. Blasko: "Position estimation in salient PM synchronous motors based on PWM excitation transients", IEEE Trans. Ind. Applicat., Vol.39, No.3, pp.835–843 (2003-5/6)

(23) M. Schroedl: "Sensorless control of AC machine at low speed and standstill based on the 'INFORM' method", in Conf. Rec. IEEE-IAS Annu. Meeting, pp.270–277 (1996)

(24) P.L. Jansen and R.D. Lorenz: "Transducerless position and velocity estimation in induction and salient AC machines", IEEE Trans. Ind. Applicat., Vol.31, No.2, pp.240–247 (1995-3/4)

(25) M.J. Corley and R.D. Lorenz: "Rotor position and velocity estimation for a salient-pole permanent magnet synchronous machine at standstill and high speeds", IEEE Trans. Ind. Applicat., Vol.34, No.4, pp.784–789 (1998-7/8)

(26) J.-I. Ha and S.-K. Sul: "Sensorless field-orientation control of an induction machine by high-frequency signal injection", IEEE Trans. Ind. Applicat., Vol.35, No.1, pp.45–51 (1999-1/2)

(27) R. Leidhold and P. Mutschler: "Improved method for higher dynamics in sensorless position detection", in Proc. IEEE IECON2008, pp.1240–1245 (2008)

(28) Y.-D. Yoon, S.-K. Sul, S. Morimoto, and K. Ide: "High bandwidth sensorless algorithm for AC machines based on square-wave-type voltage injection", IEEE Trans. Ind. Applicat., Vol.47, No.3, pp.1361–1370 (2011-5/6)

(29) R. Masaki, S. Kaneko, M. Hombu, T. Sawada, and S. Yoshihara: "Development of a position sensorless control system on an electric vehicle driven by a permanent magnet synchronous motor", in Proc. IEEE PCC Osaka 2002, Vol.2, pp.571–576 (2002)

(30) S. Kim, Y.-C. Kwon, S.-K. Sul, J. Park, and S.-M. Kim: "Position sensorless operation of IPMSM with near PWM switching frequency signal injection", in Proc. of ICPE2011-ECCE Asia (2011)

(31) S. Kim, J.-I. Ha, and S.-K. Sul: "PWM switching frequency signal injection sensorless method in IPMSM", in Proc. of ECCE, pp.3021–3028 (2011)

(32) F. Briz, M.W. Degner, P. Garcia, and R.D. Lorenz: "Comparison of saliency-based sensorless control techniques for AC machines", IEEE Trans. Ind. Applicat., Vol.40, No.4, pp.1107–1115 (2004-7/8)

(33) F. Briz, M.W. Degner, A. Diez, and R.D. Lorenz: "Static and dynamic behavior of saturation-induced saliencies and their effect on carrier-signal-based sensorless AC drives", IEEE Trans. Ind. Applicat., Vol.38, No.3, pp.670–678 (2002-5/6)

(34) D.D. Reigosa, F. Briz, M.W. Degner, P. Garcia, and J.M. Guerrero: "Temperature issues in saliency-tracking-based sensorless methods for PM synchronous machines", IEEE Trans. Ind. Applicat., Vol.47, No.3, pp.1352–1360 (2011-5/6)

(35) K. Ide, H. Iura, and M Inazumi: "Hybrid sensorless control of IPMSM Combining high frequency injection method and back EMF method", in Proc. of IECON, pp.2236–2241 (2010)

(36) Y. Jeong, R.D. Lorenz, T.M. Jahns, and S.-K. Sul: "Initial rotor position estimation of an interior permanent-magnet synchronous machine using carrier-frequency injection methods", IEEE Trans. Ind. Applicat. (2005-1/2)

(37) J.-I. Ha, K. Ide, T. Sawa, and S.-K. Sul "Sensorless rotor position estimation of an interior permanent-magnet motor from initialstates", IEEE Trans. Ind. Applicat., Vol.39, No.3, pp.761–767 (2003-5/6)

(38) S. Murakami, M. Hisatsune, T. Shiota, M. Ohto, and K. Ide: "Encoderless servo drive with adequately designed IPMSM for pulse voltage injection based position detection", in Proc. of ECCE, pp.3013–3020 (2011)

(39) J.-I. Ha: "Analysis of inherent magnetic position sensors in symmetric AC

machines for zero or low speed sensorless drives", IEEE Trans. Magn., Vol.44, No.12, pp.4689–4696 (2008-12)
(40) J.-H. Jang, S.-K. Sul, J.-I. Ha, K. Ide, and M. Sawamura: "Sensorless drive of surface-mounted permanent-magnet motor by high-frequency signal injection based on magnetic saliency", IEEE Trans. Ind. Applicat., Vol.39, No.4, pp.1031–1039 (2003-7/8)
(41) S.-C. Yang, T. Suzuki, R.D. Lorenz, and T.M. Jahns "Surface-permanent-magnet synchronous machine design for saliency-tracking self-sensing position estimation at zero and low speeds", IEEE Trans. Ind. Applicat., Vol.47, No.5, pp.2103–2116 (2011-9/10)
(42) S. Sato, H. Iura, K. Ide, and S.-K. Sul: "Three years of industrial experience with sensorless IPMSM drive based on high frequency injection method", in Proc. of Sensorless Control for Electrical Drives (SLED), pp.74–79 (2011)
(43) D.D. Reigosa, P. Garcia, D. Raca, F. Briz, and R.D. Lorenz: "Measurement and adaptive decoupling of cross-saturation effect and secondary saliencies in sensorless controlled IPM synchronous machines", IEEE Trans. Ind. Applicat., Vol.44, No.6, pp.1758–1767 (2008-11/12)
(44) M.W. Degner, and R.D. Lorenz: "Using multiple saliencies for the estimation of flux, position, and velocity in AC machines", IEEE Trans. Ind. Applicat., Vol.34, No.5, pp.1097–1104 (1998-9/10)
(45) P. Garcia, F. Briz, M.W. Degner, and D.D. Reigosa: "Accuracy, bandwidth, and stability limits of carrier-signal-injection-based sensorless control methods", IEEE Trans. Ind. Applicat., Vol.43, No.4, pp.990–1000 (2007-7/8)

Seung-Ki Sul (Member) was born in Korea in 1958. He received the B.S., M.S., and Ph.D. degrees in electrical engineering from Seoul National University, Seoul, Korea, in 1980, 1983, and 1986, respectively. From 1986 to 1988, he was an Associate Researcher with the Department of Electrical and Computer Engineering, University of Wisconsin, Madison. From 1988 to 1990, he was a Principal Research Engineer with Gold-Star Industrial Systems Company. Since 1991, he has been a member of the faculty of the Department of Electrical Engineering and Computer Science, Seoul National University, where he is currently a Professor. From 2005 to 2007, he was the Vice Dean of College of Engineering, Seoul National University. From 2008 to 2011, he was the President of Korea Electrical Engineering & Science Research Institute (KESRI). He is IEEE Fellow. His current research interests are power-electronic control of electric machines, electric/hybrid vehicle drives, and power-converter circuits.

Sungmin Kim (Non-member) was born in Seoul, Korea in 1980. He received the B.S. and M.S. degrees in electrical engineering from Seoul National University, Seoul, Korea, in 2002, 2008, respectively, where he is currently pursuing the Ph.D. degree. His current research interests are power electronics control of electric machines, sensorless drives, matrix converter drive, and power conversion circuits.